(Preprint) AAS 25-181

GOAL-ORIENTED TRAJECTORIES ABOUT MINOR BODIES USING SEQUENTIAL CONVEX PROGRAMMING: A DETERMINISTIC APPROACH

Carmine Giordano,* Stefano Campagnola,† and Francesco Topputo‡

The exploration of minor bodies offers insights into the solar system's origins and potential resources. Small satellites are becoming more appealing for close proximity mission since they are cost-effective. However, traditional trajectory design methods are labor-intensive and rigid. This paper presents a novel methodology using sequential convex programming to compute goal-oriented trajectories for spacecraft with continuous thrust systems in close proximity operations. The approach integrates engineering constraints and scientific objectives, demonstrating effectiveness through simulations of non-Keplerian and closed orbits around asteroids. The flexibility and efficiency of the method mark a significant advancement in optimal trajectory planning for minor body exploration.

INTRODUCTION

Recently, the exploration of minor bodies within the solar system has gained increasing interest due to their potential to reveal the origin of life,[1] explain the evolution of the solar system,[2] and provide resources for sustainable development of the humankind on Earth and in space.[3] On the other hand, small bodies also pose a substantial threat to life on Earth, as their impacts can cause catastrophic events.[4] For these reasons, the necessity of a thorough characterization of small bodies in terms of surface composition, internal structure, and physical features has become a primary objective in planetary science.[5] While ground-based surveys could be exploited to retrieve coarse estimates on the dimensions, shape, and rotational state, in-situ observations with robotic probes are required for detailed analyses and deeper evaluations of physical and dynamical properties.[6]

In light of this, the scientific community has prioritized missions aimed at studying minor bodies. Several spacecraft have been launched in the past to investigate both asteroids (such as OSIRIS-REx,[7] Hayabusa 2,[8] and NEAR Shoemaker[9]) and comets (like Stardust[10] and Rosetta[11]), with several others en route or planned in the next years, as Psyche[12] and RAMSES.[13] Recently, an international collaboration between NASA and ESA, the Asteroid Impact and Deflection Assessment (AIDA), has been conceived in the planetary defense framework to study the deflection capability of a kinetic impactor on potentially hazardous Near Earth Objects (NEO).[14] In this context, the secondary asteroid of the Didymos system, Dimorphos, was impacted by NASA's Double Asteroid Redirection Test (DART) spacecraft in 2022.[15] The binary system will be visited again in 2027

*PostDoc Fellow, Department of Aerospace Science and Technology, Politecnico di Milano, via La Masa, 34, Milan, 20156, Italy.

†Europa Clipper Mission Design Manager, Outer Planet Mission Analysis Group, Jet Propulsion Laboratory, California Institute of Technology, Pasadena, California, 91109.

‡Full Professor, Department of Aerospace Science and Technology, Politecnico di Milano, via La Masa, 34, Milan, 20156, Italy.

by ESA's Hera mission, that will carry out scientific investigation on the dynamical and physical properties of the binary system, and their changes after the impact.[16]

Alongside large-scale missions, in recent times, there has been an increasing momentum in employing small platforms, such as CubeSats and SmallSats, in order to get considerable scientific return at significantly lower costs.[17,18] Notably, both DART and Hera have carried and released CubeSats in situ (LICIACube,[19] and Juventas[20] and Milani,[21] respectively), with the aim to support scientific observations. Additionally, concepts of standalone small satellites, reaching a target minor body departing from the Earth, have been devised. However, due to their limited size and mass constraints, miniaturized probes often rely on electric propulsion systems to maximize efficiency and minimize the propellant mass to be embarked.[22,23]

Traditionally, the conventional approach to design trajectories for remote-sensing missions in close proximity operations (CPOs) about minor bodies has been either to fly long-term stable orbits[12,20] or identify scientifically valuable points and manually connect them to design the trajectory.[24–26] In the former case, closed trajectories requiring minimum orbit maintenance are exploited, even though finding them could be challenging due to the extremely chaotic environments. Additionally, they have limited flexibility in terms of illumination and range, affecting the potential scientific return in case of remote-sensing passive payloads. In the latter case, the trajectory design is labor-intensive, time-consuming, and requires extensive human intervention. To address these challenges, goal-oriented approaches have recently emerged, wherein high-level mission objectives are provided to an algorithm that autonomously computes the trajectory within a continuous replanning framework to best achieve the desired scientific goals. Surovik and Scheeres[27] introduced this concept by applying heuristic-guided reachability analyses in a receding horizon scheme, enabling the design of trajectories with impulsive orbit control maneuvers that meet abstractly specified science goals. Reachability maps, which represent the regions of space a spacecraft can access from a given maneuver point based on its propulsion capabilities and mission constraints, play a key role in this process by guiding the algorithm in identifying feasible paths. This methodology was later expanded to perform a global mapping of a minor body[28] and to address both stringent engineering and scientific constraints for binary asteroid exploration.[29]

Despite their potential, current goal-oriented approaches depend on reachability maps. While robust and suitable to be applied to onboard planning, they can be limiting for platforms equipped with continuous thrust systems.

In this work, a novel methodology to compute goal-oriented trajectories around minor bodies is presented, with special interest in small platforms utilizing continuous thrust. This approach solves the nonlinear optimal control problem for goal-oriented trajectory design by leveraging on sequential convex programming (SCP),[30] aiming to compute optimal trajectories that satisfy both engineering constraints and scientific goals. Additionally, the approach automates the selection of the mission objectives to be fulfilled by determining within the optimization algorithm which targets can be met and when, streamlining the trajectory design process. The use of SCP is particularly advantageous as it reduces the complexity of the problem to solving mixed-integer second-order cone programs rather than a more challenging mixed-integer nonlinear program, and it has the ability to efficiently handle nonconvex optimal control problems with nonlinear dynamics and constraints, as shown in various aerospace contexts, such as powered descent guidance[31] and low-thrust trajectory optimization.[32,33] As a matter of fact, by breaking down the problem into simpler convex subproblems, SCP enhances numerical tractability compared to directly solving the full nonlinear problem.

Different discretization techniques, thrust region methods, and scientific constraints formulations are applied to the methodology and then compared by performing numerical simulations in two different scenarios: a non-Keplerian trajectory about a small asteroid, and a closed orbit about a bigger minor body. Lastly, the flexibility of the methodology is demonstrated by applying it to an alternative formulation for the scientific constraints and to different sets of constraints.

BACKGROUND

Goal-oriented trajectory design

The goal-oriented trajectory design problem has the aim to find a trajectory close to a minor body satisfying all the scientific targets in a given timeframe. Scientific objectives can be described as high-level functions that must be respected at least in a single point along the path. These objectives can represent a range of potential scientific goals, depending on the mission's overall purpose, e.g., flybys at specific altitude and latitude for gravity or radio science, or high-phase limb observations to study the atmosphere. Without loss of generality, the scientific objectives in this work focus on remote-sensing observations using passive payloads to observe features on the minor body. Specifically, in this work, the scientific merit is measured by the number of successful observations of features located within a conical region, with the cone centered nadir to the spacecraft and having a width equal to the field of view. This formulation inherently constrains the spacecraft attitude and assumes no use of mirrors or gimbals. These assumptions not only are common in the goal-oriented settings,[27,29] but they are also particularly reasonable for small satellites, where passive payloads are favored for their lower power consumption, and the exclusion of mirrors or gimbals helps minimize mass and avoid the complexities associated with mechanical systems.
As consequence, each scientific target can be represented as mathematically as conical frusta (Fig. 1), which allows to observe the specific feature a) within a given range, to respect a desired ground sampling distance and avoid safety concerns; b) within a certain angle from the normal, to have a clear view of the feature.

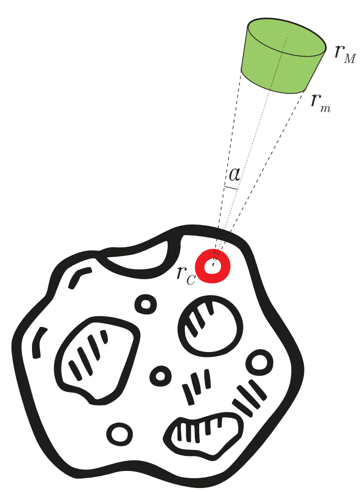

Figure 1: Representation of scientific goal. The green volume is the target region.

The mathematical representation of this kind of scientific targets is[29]

$$r_m \leq \|\mathbf{r}(t_k) - \mathbf{r}_{c_i}(t_k)\| \leq r_M \tag{1a}$$

$$\frac{\mathbf{r}(t_k) \cdot \mathbf{r}_{c_i}(t_k)}{\|\mathbf{r}(t_k)\|\|\mathbf{r}_{c_i(t_k)}\|} \leq \cos\alpha \tag{1b}$$

where $\mathbf{r}$ is the position of the spacecraft at the given time t_k and the i-th scientific target is described by the position of the feature r_{c_i}, the minimum and maximum distance from the feature, r_m and r_M, respectively, and the semi-aperture of the conical frustum α.

Sequential convex programming

Sequential convex programming is a powerful method for solving optimal control problem by transforming nonconvex problems into a series of easier-to-solve convex subproblems. This approach allows efficient handling of complex dynamics and constraints, making it particularly useful for optimizing continuous-thrust trajectories. The efficiency and flexibility of SCP have made this approach popular in various aerospace contexts, such as powered descent guidance[31] and interplanetary trajectory design.[32, 33]
In order to understand how SCP is currently exploited, a generic low-trust optimal control problem can be considered. It can be formalized as

$$\underset{\mathbf{u}(t)}{\text{Minimize}}\; J := -m(t_f) \tag{2}$$

subject to

$$\begin{cases} \dot{\mathbf{r}} = \mathbf{v} \\ \dot{\mathbf{v}} = \mathbf{f}_f(\mathbf{x}, t) + \frac{\mathbf{T}(t)}{m(t)} \\ \dot{m} = -\frac{\|\mathbf{T}(t)\|}{I_{sp} g_0} \end{cases}, \qquad \mathbf{x}(t_0) = \mathbf{x}_0 \tag{3}$$

and

$$0 \leq \|\mathbf{T}(t)\| \leq T_{\max} \tag{4}$$

where $\mathbf{x} = [\mathbf{r}, \mathbf{v}, m]^T$ is the state, embedding the position, the velocity, and the mass, respectively, $\mathbf{T}$ is the thrust vector and $T_{\max}$ its attainable maximum value, I_{sp} the thruster specific impulse, and g_0 gravitational acceleration at sea level. The term $\mathbf{f}_f(\mathbf{x}, t)$ represents the free-body dynamics.

Decoupling states and control In this context, the first step to be performed in order to facilitate the problem solution in a SCP setting is to eliminate the coupling between state and control in Eqs. (3) by defining two new control variables, and a different metric for the mass[36]

$$\Gamma(t) = \frac{\|\mathbf{T}(t)\|}{m(t)}, \quad \boldsymbol{\tau}(t) = \frac{\mathbf{T}(t)}{m(t)}, \quad z(t) = \ln(m(t))$$

In this case, the equations of motion become

$$\begin{cases} \dot{\mathbf{r}} = \mathbf{v} \\ \dot{\mathbf{v}} = \mathbf{f}_f(\mathbf{x}, t) + \boldsymbol{\tau}(t) \\ \dot{z} = -\frac{\Gamma(t)}{I_{sp} g_0} \end{cases} \tag{5}$$

Additionally, in order to assure compatibility among the new variables, the constraint

$$\|\boldsymbol{\tau}(t)\| = \Gamma(t) \tag{6}$$

is added, while Eq. (4) in the new variables is

$$0 \leq \Gamma(t) \leq T_{\max} e^{-z(t)} \tag{7}$$

Convexification Then, Eqs. (5) is linearized about a reference solution $(\bar{\mathbf{x}}, \bar{\mathbf{u}})$, with the control vector defined as $\mathbf{u} = [\boldsymbol{\tau}, \Gamma]^T$, and a trust-region constraint is added to keep the linearization valid.[30] Thus, the convexified optimization problem for a generic continuous-thrust problem is

$$\underset{\mathbf{u}(t)}{\text{Minimize}}\, J := -z(t_f) + \lambda \|\boldsymbol{\nu}(t)\|_1 + \lambda \sum_{j \in \text{Ineq}} \max\left(0, \eta_j(t)\right) \tag{8}$$

subject to

$$\dot{\mathbf{x}} = \mathbf{f}(\bar{\mathbf{x}}(t), \bar{\mathbf{u}}(t)) + A(\mathbf{x}(t) - \bar{\mathbf{x}}(t)) + B(\mathbf{u}(t) - \bar{\mathbf{u}}(t)) + \boldsymbol{\nu}(t), \qquad \mathbf{x}(t_0) = \mathbf{x}_0 \tag{9}$$

and

$$0 \leq \Gamma(t) \leq T_{\max} e^{-\bar{z}(t)} \left(1 - z(t) + \bar{z}(t)\right) + \eta_1(t) \tag{10}$$

$$\|\boldsymbol{\tau}(t)\| \leq \Gamma(t) \tag{11}$$

and

$$\|\mathbf{x}(t) - \bar{\mathbf{x}}(t)\|_1 \leq R \tag{12}$$

where

$$A = \left.\frac{\partial \mathbf{f}}{\partial \mathbf{x}}\right|_{\bar{\mathbf{x}}(t)}, \quad B = \left.\frac{\partial \mathbf{f}}{\partial \mathbf{u}}\right|_{\bar{\mathbf{u}}(t)}$$

The variables $\boldsymbol{\nu}$ and $\eta(t)$ are the virtual controls and are added to avoid artificial infeasibility, while artificial unboundeness is managed by imposing a constraint on the trust region radius R (Eq. (12)). Eq. (11) is the convex relaxation of Eq. (6), while Eq. (10) is the linearization about the reference solution of the non-convex constraints in Eq. (7).
Problem in Eqs. (8)–(12) is solved than iteratively until certain stopping criteria are met.[30]

PROBLEM FORMULATION

The generic formulation for the low-thrust fuel-optimal problem can be specialized by considering the scientific goals. Given a spacecraft equipped with low thrust propulsion system flying close to a minor body, the goal-oriented minimum-fuel problem has the aim to find a trajectory satisfying all the scientific targets in a given timeframe while minimizing the use of propellant. The goal-oriented minimum-fuel problem can be formalized as

Problem 1 (General deterministic goal-oriented minimum-fuel problem)**.**

$$\underset{\mathbf{u}(t)}{\text{Minimize}}\, J := -z(t_f)$$

subject to

Eqs. (5)–(7)

and N_g scientific constraints

$$\text{Eqs. (1)} \qquad \text{for some } t_k \in [t_0, t_f], \qquad \text{for } i = 1, \dots, N_g$$

Additionally, the free dynamics term $\mathbf{f}_f$ in Eq. (5) is specialized for close proximity of a minor body. A non-inertial body fixed frame is considered. This choice allows to have the feature positions to be fixed, independent of the time, and ease the implementation of Eqs. (1). Thus, defying $\boldsymbol{\omega}$ as the angular velocity of the main body,

$$\mathbf{f}_f(\mathbf{x}, t) = \mathbf{f}_g(\mathbf{r}, t) + \underbrace{\sum_{k \in \mathcal{P}} -\mu_k \left(\frac{\mathbf{r}_k}{\|\mathbf{r}_k\|^3} + \frac{\mathbf{r} - \mathbf{r}_k}{\|\mathbf{r} - \mathbf{r}_k\|^3} \right)}_{\text{3-body acc.}} + \underbrace{C_r \frac{A}{m} \frac{P_0 d_0^2}{c} \frac{\mathbf{r} - \mathbf{r}_S}{\|\mathbf{r} - \mathbf{r}_S\|^3}}_{\text{SRP}} - \boldsymbol{\omega} \times (\boldsymbol{\omega} \times \mathbf{r}) - 2\boldsymbol{\omega} \times \mathbf{v} \tag{13}$$

where $\mathcal{P}$ is the set containing third bodies acting on the spacecraft and characterized by the gravitational parameter μ_k and relative position with respect to minor body $\mathbf{r}_k$. The solar ration pressure (SRP) is computed exploiting the canonball model, with P_0 ($1367\,\mathrm{W/m^2}$) the solar flux at 1 astronomical unit (AU), c is the speed of light, d_0 is the Sun–Earth distance (1 AU), C_r is the reflectivity coefficient of the spacecraft, A is its equivalent surface area, and $\mathbf{r}_S$ the position of the Sun.
The term $\mathbf{f}_g(\mathbf{r}, t)$ represents the gravitational acceleration exerted by the main body. Considering the complex shapes of minor bodies, the use of the simple point-body model could produce inaccurate results. For this reason, in this work, two more complex models will be used to compute the gravitational field of the main body, that are, the *tri-axial ellipsoid model* with[34]

$$\mathbf{f}_g(\mathbf{r}, t) = -\frac{3}{2}\mu \begin{bmatrix} \tilde{x} \int_\lambda^\infty \frac{1}{(a^2+u)\Delta(u)}\,\mathrm{d}u \\ \tilde{y} \int_\lambda^\infty \frac{1}{(b^2+u)\Delta(u)}\,\mathrm{d}u \\ \tilde{z} \int_\lambda^\infty \frac{1}{(c^2+u)\Delta(u)}\,\mathrm{d}u \end{bmatrix} \tag{14}$$

where a, b, and c are the semi-axes of the ellipsoid, in decreasing order, $\tilde{x}$, $\tilde{y}$, and $\tilde{z}$ the Cartesian components of position relative vector with respect to the ellipsoid (i.e., $\tilde{\mathbf{r}} = \mathbf{r} - \mathbf{r}_{ell}$), and $\Delta(u) = \sqrt{(a^2+u)\,(b^2+u)\,(c^2+u)}$; and the *spherical harmonics model* with[35]

$$\mathbf{f}_g(\mathbf{r}, t) = -\nabla V \tag{15}$$

where V is the main body's gravitational potential

$$V = -\frac{\mu}{r} \left(1 + \sum_{n=2}^{N_z} \frac{R^n J_n P_n^0(\sin\theta)}{r^n} + \sum_{n=2}^{N_t} \sum_{m=1}^{n} \frac{R^n P_n^m(\sin\theta)\,(C_n^m \cos m\phi + S_n^m \sin m\phi)}{r^n} \right) \tag{16}$$

with (r, θ, ϕ) the spherical coordinates associated to the position $\mathbf{r}$, R the body reference radius, P_n^m the associated Legendre functions of degree n and order m, and J_n, and C_n^m and S_n^m the dimensionless zonal and tesseral coefficients, respectively. The use of a body-fixed reference frame is also useful to ease the evaluation of the gravitational acceleration in both the models.

Convexification

Then, Problem 1 is convexified to be exploited in the SCP framework. A convex goal-oriented minimum-fuel problem can be formalized as

Problem 2 (Convexified goal-oriented minimum-fuel problem)**.**

$$\underset{\mathbf{u}(t)}{\text{Minimize}}\, J := \text{Eq. (8)}$$

subject to

$$\text{Eqs. (9)–(12)}$$

and N_g scientific constraints

$$\begin{cases} -\dfrac{(\bar{\mathbf{r}}(t_k) - \mathbf{r}_{c_i}) \cdot \mathbf{r}(t_k)}{\|\bar{\mathbf{r}}(t_k) - \mathbf{r}_{c_i}\|} \leq (r_m - \|\bar{\mathbf{r}}(t_k) - \mathbf{r}_{c_i}\|) + \eta_2(t) & \quad (17a) \\ \|\mathbf{r}(t_k) - \mathbf{r}_{c_i}\| \leq r_M \qquad \text{for some } t_k \in [t_0, t_f], \qquad \text{for } i = 1, \dots, N_g & \quad (17b) \\ \|\mathbf{r}(t_k) - \mathbf{r}_{c_i}\| \leq \dfrac{1}{\cos\alpha} \left(\mathbf{n}_i^T \mathbf{r}(t_k) - \mathbf{n}_i^T \mathbf{r}_{c_i}\right) & \quad (17c) \end{cases}$$

where Eq. (17a) is the linearization about the reference solution of the non-convex constraints in Eq. (1a), and Eq. (1b) has been re-arranged in Eq. (17c), with $\mathbf{n}_i = \mathbf{r}_{c_i}/\|\mathbf{r}_{c_i}\|$, to highlight that is a second-order cone constraint.

Discretization

The convexified problem must be translated in a convex programming problem to be solved. In order to do so, the timespan $[t_0, t_f]$ is subdivided into N segments, and both the state and the control are projected into this time grid to have finite-dimensional variables.

However, it could be noted that the scientific targets are still defined in a fuzzy way, since the time at which Eqs. (17) must be satisfied could be any value inside the defined timeframe. If the discretization is considered, this could be translated in the scientific targets to be satisfied at at least one discretization point. This kind of constraints could be easily handled by using the Big M method.

Hence, Problem 2 is converted in the following mixed-integer second-order cone constraint problem (MISOCP)

Problem 3 (Convex programming problem for the goal-oriented minimum-fuel problem)**.**
Find $\mathbf{y} = [\mathbf{x}_k, \mathbf{u}_k, \boldsymbol{\nu}_k, \eta_k, \gamma_k],\ k = 1, \dots, N$, such that

$$J := -z_N + \sum_{i=0}^{N} \lambda \|\boldsymbol{\nu}_k\|_1 + \sum_{i=0}^{N} \lambda \max(0, \eta_k) \tag{18}$$

is minimized, subject to

$$\boldsymbol{\Delta} = \hat{A}\mathbf{x} + \hat{B}\mathbf{u} + \mathbf{q} + \hat{N}\boldsymbol{\nu} = \mathbf{0} \tag{19}$$

the control constraints

$$0 \leq \Gamma_k \leq T_{\max} e^{-\bar{z}_k} (1 - z_k + \bar{z}_k) + \eta_{1,k} \tag{20}$$

$$\|\boldsymbol{\tau}_k\| \leq \Gamma_k \tag{21}$$

and the goal constraints

$$
\begin{cases}
-\dfrac{(\bar{\mathbf{r}}_k - \mathbf{r}_{c_i}) \cdot \mathbf{r}_k}{\|\bar{\mathbf{r}}_k - \mathbf{r}_{c_i}\|} - (r_m - \|\bar{\mathbf{r}}(t_i) - \mathbf{r}_{c_i}\|) - \eta_{2,k} \leq M(1 - \gamma_{i,k}) & \quad (22a) \\
\|\mathbf{r}_k - \mathbf{r}_{c_i} - r_M\| \leq M(1 - \gamma_{i,k}) & \quad (22b) \\
\|\mathbf{r}_k - \mathbf{r}_{c_{i,k}}\| - \left(\dfrac{1}{\cos\alpha}(\mathbf{n}^T\mathbf{r}_k - \mathbf{n}^T\mathbf{r}_{c_i})\right) \leq M(1 - \gamma_{i,k}) \qquad \text{for } i = 1, \ldots, N_g & \quad (22c) \\
\displaystyle\sum_{k=0}^{N} \gamma_{i,k} \geq 1 & \quad (22d)
\end{cases}
$$

and the trust region constraint

$$
\|\mathbf{x} - \bar{\mathbf{x}}\|_1 \leq R \tag{23}
$$

Eq. (19) represents the general formulation of the dynamical defects related to a generic discretization method, with $\mathbf{q}$ being a constant value. A detailed discussion on this is given in the next section. The variable $\gamma_{i,k}$ is the index binary variable for the single scientific target, i.e., it is 1 if the target i is respected at point k, and 0 otherwise, with M a sufficiently large value. Eq. (22d) has been added to guarantee that each scientific constraint is satisfied at least once in the given timeframe.

PROBLEM IMPLEMENTATION

Discretization methods

The choice of the best suitable discretization method is not straightforward and usually it can be determined only by performing numerical simulations of the problem under analysis. Comparison of different techniques have been investigated both for the PDG[37] and the LTO.[33] However, these results cannot be extended to the close-proximity goal-oriented problem due not only to different dynamics and time horizon, but especially to the different nature of the discretized scientific constraints.

The most commonly used discretization techniques in trajectory optimization are collocation and control interpolation methods.[38] Collocation methods parameterize both state and control variables using specific basis functions, while control interpolation methods focus solely on parameterizing the control history. Both types have been used successfully for trajectory optimization in space applications exploiting SCP. Considering the most common choices in previous works,[33,37] the discretization methods considered in this paper are:

1. An arbitrary-order Hermite Legendre–Gauss–Lobatto collocation method;

2. An adaptive Legendre–Gauss–Radau pseudospectral collocation method;

3. Zeroth- and First-Order Hold control interpolation methods.

Arbitrary-order Hermite Legendre–Gauss–Lobatto method The arbitrary-order Hermite Legendre–Gauss–Lobatto (LGL) discretization is a generalization of the Hermite–Simpson method.[39] It has been used extensively both in direct nonlinear transcription[40,41] and in sequential convex programming frameworks.[42]

In this case, the trajectory is divided in N segments. In each segment, the state and the controls are approximated as n-th order polynomials, with n the selected order of the LGL,

$$\mathbf{x}_k(\xi) = \sum_{j=0}^{n} \mathbf{a}_j^{(k)} \xi^j, \qquad \mathbf{u}_k(\xi) = \sum_{j=0}^{(n+1)/2} \mathbf{c}_j^{(k)} \xi^j \tag{24}$$

where $\xi \in [-1, 1]$ is the scaled nondimensional time in each segment, i.e.,

$$\xi = 2\frac{t}{h} - \frac{t_{k+1} + t_k}{h}$$

where $h = t_{k+1} - t_k$ is the time step, and $\mathbf{a}_j^{(k)}$ and $\mathbf{c}_j^{(k)}$ are the state and control coefficients of the k-th segment. Nodes θ and collocation points ζ are the odd and even roots, respectively, of the $(n-1)$-th degree Legendre polynomial derivative.[39]

For each segment, the state coefficients can be retrieved by exploiting the information at the nodes, solving the linear system[40]

$$\Theta \mathbf{a} = \mathbf{b} \tag{25}$$

where

$$\Theta = \begin{bmatrix} I_{n_x} & \theta_1 I_{n_x} & \theta_1^2 I_{n_x} & \dots & \theta_1^n I_{n_x} \\ \vdots & \vdots & \vdots & \ddots & \vdots \\ I_{n_x} & \theta_{n_p} I_{n_x} & \theta_{n_p}^2 I_{n_x} & \dots & \theta_{n_p}^n I_{n_x} \\ 0_{n_x} & I_{n_x} & 2\theta_1 I_{n_x} & \dots & n\theta_1^{n-1} I_{n_x} \\ \vdots & \vdots & \vdots & \ddots & \vdots \\ 0_{n_x} & I_{n_x} & 2\theta_{n_p} I_{n_x} & \dots & n\theta_{n_p}^{n-1} I_{n_x} \end{bmatrix}$$

$$\mathbf{a} = [\mathbf{a}_0, \dots, \mathbf{a}_n]^T$$

and

$$\mathbf{b} = \left[\mathbf{x}(\theta_1), \dots, \mathbf{x}(\theta_{n_p}), \frac{h}{2}\mathbf{f}_l(\theta_1), \dots, \frac{h}{2}\mathbf{f}_l(\theta_{n_p})\right]^T$$

with $n_p = (n+1)/2$ the number of nodes in each segment, I_{n_x} the n_x-dimensional identity matrix, 0_{n_x} the $n_x \times n_x$ null matrix, ad $\mathbf{f}_l$ the linearized dynamics in Eq. (9). Once the coefficients are retrieved, the state at the collocation points can be defined by interpolation

$$\mathbf{x}(\zeta) = Z\mathbf{a} = Z\Theta^{-1}\mathbf{b} = H\mathbf{b} \tag{26}$$

with

$$Z = \begin{bmatrix} I_{n_x} & \zeta_1 I_{n_x} & \zeta_1^2 I_{n_x} & \dots & \zeta_1^n I_{n_x} \\ \vdots & \vdots & \vdots & \ddots & \vdots \\ I_{n_x} & \zeta_{n_c} I_{n_x} & \zeta_{n_c}^2 I_{n_x} & \dots & \zeta_{n_c}^n I_{n_x} \end{bmatrix}$$

where $n_c = (n-1)/2$ the number of collocation points in each segment. Similarly, the derivative of the state at the collocation points is

$$\frac{\mathrm{d}\mathbf{x}(\zeta)}{\mathrm{d}\xi} = \mathbf{a} = Z'\Theta^{-1}\mathbf{b} = H'\mathbf{b} \tag{27}$$

with

$$Z' = \begin{bmatrix} 0_{n_x} & I_{n_x} & 2\zeta_1 I_{n_x} & \dots & n\zeta_1^{n-1} I_{n_x} \\ \vdots & \vdots & \vdots & \ddots & \vdots \\ 0_{n_x} & I_{n_x} & 2\zeta_{n_c} I_{n_x} & \dots & n\zeta_{n_c}^{n-1} I_{n_x} \end{bmatrix}$$

Exploiting the same procedure, the control at the collocation points is[42]

$$\mathbf{u}\left(\zeta\right) = H_u \mathbf{u} \tag{28}$$

Combining all this quantities in a single equation, the dynamics constraints for each segment can be computed as[42]

$$\boldsymbol{\Delta} = H'\mathbf{b} - \frac{h}{2}\left[\mathbf{f}_f + A\left(H\mathbf{b} - H\bar{\mathbf{b}}\right)\right] + BH_{\mathbf{u}}\mathbf{u} + \boldsymbol{\nu} = 0 \tag{29}$$

Legendre–Gauss–Radau Pseudospectral method Pseudospectral methods (PS) exploit pseudospectral theory to solve optimal control problems.[43] They have been proven to be fast and efficient to solve nonlinear spacecraft trajectory optimization since they enjoy the spectral convergence.[44] They have also been adapted to SCP.[45] However, while global PS, i.e., with a single interpolating function across the whole time horizon, are usually exploited in nonlinear settings, adaptive PS, i.e., with piecewise polynomials, are preferred in SCP, since they are characterized by sparse matrices.[32]
In the Legendre–Gauss–Radau PS method, for each segment, the state and the controls are approximated as polynomials

$$\mathbf{x}_k(\xi) = \sum_{j=0}^{n} \mathbf{x}_j L^j(\xi), \qquad \mathbf{u}_k(\xi) = \sum_{j=0}^{n} \mathbf{u}_j L^j(\xi) \tag{30}$$

where $\xi \in [-1, 1]$ is the scaled nondimensional time in each segment, and

$$L_j(\xi) = \prod_{\substack{l=0 \\ l\neq j}}^{n} \frac{\xi - \xi_l}{\xi_k - \xi_l} \tag{31}$$

Collocation points are selected as the roots of the polynomial $P_{n-1} + P_n$, where P_n is the n-th degree Legendre polynomial.
The basic idea of pseudospectral methods is to approximate the differential operator $\dot{\mathbf{x}}_k = D_k \mathbf{x}_k$, where D is the differentiation matrix defined as $D_{ij} = L_j'(\xi_i)$. While the standard PS is suitable for trajectory optimization with SCP, its equivalent integral formulation have shown better performances.[46] In this case, the dynamical constraints at each collocation point i within a segment can be computed as[32]

$$\mathbf{x}_i - \left(\mathbf{x}_k + \frac{h}{2}\sum_{j=0}^{n-1} I_{ij}\left(A\left(\mathbf{x}_j - \bar{\mathbf{x}}_j\right) + B\mathbf{u}_j + \mathbf{f}_f\left(\bar{\mathbf{x}}_j, \bar{\mathbf{u}}_j\right) + \boldsymbol{\nu}_j\right)\right) = \mathbf{0} \tag{32}$$

with I the integration matrix defined as $I = \hat{D}^{-1}$, with $\hat{D}$ the matrix D without the first column.

Zeroth- and First-Order Hold In the first-order hold (FOH) method, the control history is approximated as a piecewise affine function, that is[30]

$$\mathbf{u}(t) = \frac{t_{k+1} - t}{h}\mathbf{u}_k + \frac{t - t_k}{h}\mathbf{u}_{k+1} = \lambda^-(t)\mathbf{u}_k + \lambda^+(t)\mathbf{u}_{k+1} \tag{33}$$

In this case, the linearized dynamics in Eq. (9) becomes

$$\dot{\mathbf{x}} = A\mathbf{x} + B\lambda^-\mathbf{u}_k + B\lambda^+\mathbf{u}_{k+1} + \left(\mathbf{f}_f\left(\bar{\mathbf{x}}, \bar{\mathbf{u}}\right) - A\bar{\mathbf{x}}\right) \tag{34}$$

In each segment, Eq. (34) could be integrated by exploiting the linear systems theory. Thus, the dynamical constraint for each segment become[30]

$$\mathbf{x}_{k+1} - \left(\hat{A}_k \mathbf{x}_k + \hat{B}_k^- \mathbf{u}_k + \hat{B}_k^+ \mathbf{u}_{k+1} + \mathbf{q}_k + \boldsymbol{\nu}_k\right) = \mathbf{0} \tag{35}$$

where

$$\begin{aligned}
\hat{A}_k &= \Phi(t_k, t_{k+1}) \\
\hat{B}_k^- &= \hat{A}_k \int_{t_k}^{t_{k+1}} \Phi^{-1}(t_k, t) B \lambda^- \, \mathrm{d}t \\
\hat{B}_k^+ &= \hat{A}_k \int_{t_k}^{t_{k+1}} \Phi^{-1}(t_k, t) B \lambda^+ \, \mathrm{d}t \\
\mathbf{q}_k &= \hat{A}_k \int_{t_k}^{t_{k+1}} \Phi^{-1}(t_k, t) \left(\mathbf{f}_f\left(\bar{\mathbf{x}}, \bar{\mathbf{u}}\right) - A_k \bar{\mathbf{x}}\right) \, \mathrm{d}t
\end{aligned}$$

where $\Phi(t_k, t)$ is the state transition matrix between time t_k and time t.
In zeroth-order hold (ZOH) method the control is considered constant for each interval, i.e.,

$$\mathbf{u}(t) = \mathbf{u}_k, \qquad \forall t \in [t_k, t_{k+1}] \tag{36}$$

So, dynamics constraints can be written in the same way as Eq. (35), but in this case $\hat{B}_k^+ = 0$, while $\hat{B}_k^- = \hat{A}_k \int_{t_k}^{t_{k+1}} \Phi^{-1}(t_k, t) B \, \mathrm{d}t$.

Trust region approaches

In SCP it is of paramount importance having a mechanism that imposes a constraint on the trust region and manage its radius. At each iteration, the solution of the convex solver is accepted or rejected based on the following ratio[30]

$$\rho = \frac{\bar{\phi} - \phi}{\bar{\phi} - \theta} \tag{37}$$

where

$$\phi = -z_N + \sum_{j \in I_{eq}} \lambda_j \|\mathbf{h}_j\|_1 + \sum_{j \in I_{ineq}} \lambda_j \max(0, g_j) \tag{38}$$

is the actual cost, with $\mathbf{h}$ and g are the constraint violation of the equality and inequality constraints of the non-convex problem, respectively, and

$$\theta = -z_N + \sum_{j \in I_{eq}} \lambda_j \|\boldsymbol{\nu}_j\|_1 + \sum_{j \in I_{ineq}} \lambda_j \max(0, \eta_j) \tag{39}$$

is the predicted cost reduction. Generally speaking, if $\rho \ll 1$, the actual costs decrease is smaller that the predicted one, so the linearized problem is performing poorly, so the solution must be rejected and the radius reduced, while if $\rho \simeq 1$, the actual costs and the predicted ones are similar, so the linearized problem is representing properly the nonlinear one, the step must be accepted and, in case, the radius increased. In this work, two mechanisms, being a hard and a soft approach, to handle the trust region will be investigated. The difference between hard and soft trust region lies in the way of dealing with artificial unboundness and the constraint given by Eq. (23).

Hard trust region approach With the hard trust region approach, the trust region constraint in Eq. (23) is directly used. In this case, three parameters (ρ_0, ρ_1, ρ_2), with $\rho_0 < \rho_1 < \rho_2$, are selected and used to manage the trust region. If $\rho \leq \rho_0$, the step is rejected and a smaller new region radius R is selected. Otherwise, the solution is accepted and the trust region is updated as[30]

$$R = \begin{cases} R/\alpha & \text{if} \quad \rho_0 \leq \rho < \rho_1 \\ R & \text{if} \quad \rho_1 \leq \rho < \rho_2 \\ \beta R & \text{if} \quad \rho \geq \rho_2 \end{cases} \tag{40}$$

with α and β predetermined values grater than 1.

Soft trust region approach For the soft trust region approach, the constrain in Eq.(23) is not imposed directly, but a penalty function is added to the performance index,[33] i.e.,

$$\hat{J} = J + \lambda_{TR} \max(0, \|\mathbf{x}_k - \bar{\mathbf{x}}_k\|_1 - R) \tag{41}$$

In this case, the trust region update mechanism defines first the metric

$$g = \|\mathbf{x}_k - \bar{\mathbf{x}}_k\|_1 - R \tag{42}$$

then, if $g > 0$, the step is rejected and $\lambda_{TR} = \tau\lambda_{TR}$ with $\tau > 1$. Otherwise, the same rule in Eq. (40) is applied.

Target constraints approaches

Two different approaches can be used also for the target constraints, and specifically in the way of dealing with the indexing constraint in Eq. (22d).
In the case of a hard scientific constraints approach, Eq. (22d) is imposed directly in the optimization problem. On the other hand, for the soft scientific constraint approach, Eq. (22d) is not considered. Instead, the performance index is modified with a rewarding function

$$\hat{J} = J - \lambda_g \sum_{i=1}^{N_g} \min\left(1, \sum_{k=0}^{N} \gamma_{i,k}\right) \tag{43}$$

This rewarding function is designed to be 0 whenever the goal is not reached and it decreases with the number of nodes satisfying the goal, being $-\lambda_g$ when all the targets are satisfied at least once.
The two approaches, however, can be applied in different situation, based on the aim of the optimization problem. Indeed, the use of hard goals is preferable only when it is mandatory to satisfy all the targets, since this approach fails when fulfilling all the goals is not feasible. On the other hand, the soft approach is able to generate always a feasible solution, but it is not given that all the targets are satisfied and it could be a more cumbersome problem to solve since the cost function becomes piecewise continuous.

NUMERICAL SIMULATIONS

The performances of the SCP algorithm to solve the goal-oriented problem about a minor body are evaluated by means of several numerical simulations. In SCP, the basic algorithm foresees to solve the convex programming problem (Problem 3) recursively. However, MISOCPs are usually more difficult to solve than simple SOCPs. For this reason, it is preferable to reduce the times the

MISOCP is solved. The this aim the procedure in Fig. 2 is exploited. The MISOCP is solved iteratively until the nonlinear constraint metric $\|\mathbf{h}\|_\infty$, with $\mathbf{h}$ the collection of Eqs. (6), (7), and (1) evaluated in the nodal points, is below a certain threshold $\bar{h}$. When this condition is satisfied, meaning that we are close to the solution of the nonlinear problem, the binary variable γ is fixed and so a simple SOCP is solved in the following iterations. In this way, a smaller number of mixed-integer problems are solved and the computational burden reduced. However, $\bar{h}$ must be selected carefully, since high values reduce the number of mixed-integer iterations, but can affect the convergence, while low values can increase significantly the runtime.

Iterations are stopped successfully if the maximum nonlinear constraint violation and the improvement of the modified mass metric are below a certain threshold, i.e, $\|\mathbf{h}\|_1 \leq \varepsilon_h$ and $\bar{z} - z \leq \varepsilon_z$. On the other hand, the procedure is terminated without success if the relative difference of the solution vector in two consecutive iterations is below a certain threshold (i.e., $\|\bar{x} - x\|_1 \leq \varepsilon_x$), meaning that there is not any improvement in the solution, or if the trust region radius is too small (i.e., $R \leq \varepsilon_R$). All these relevant parameter are provided in Table 1.

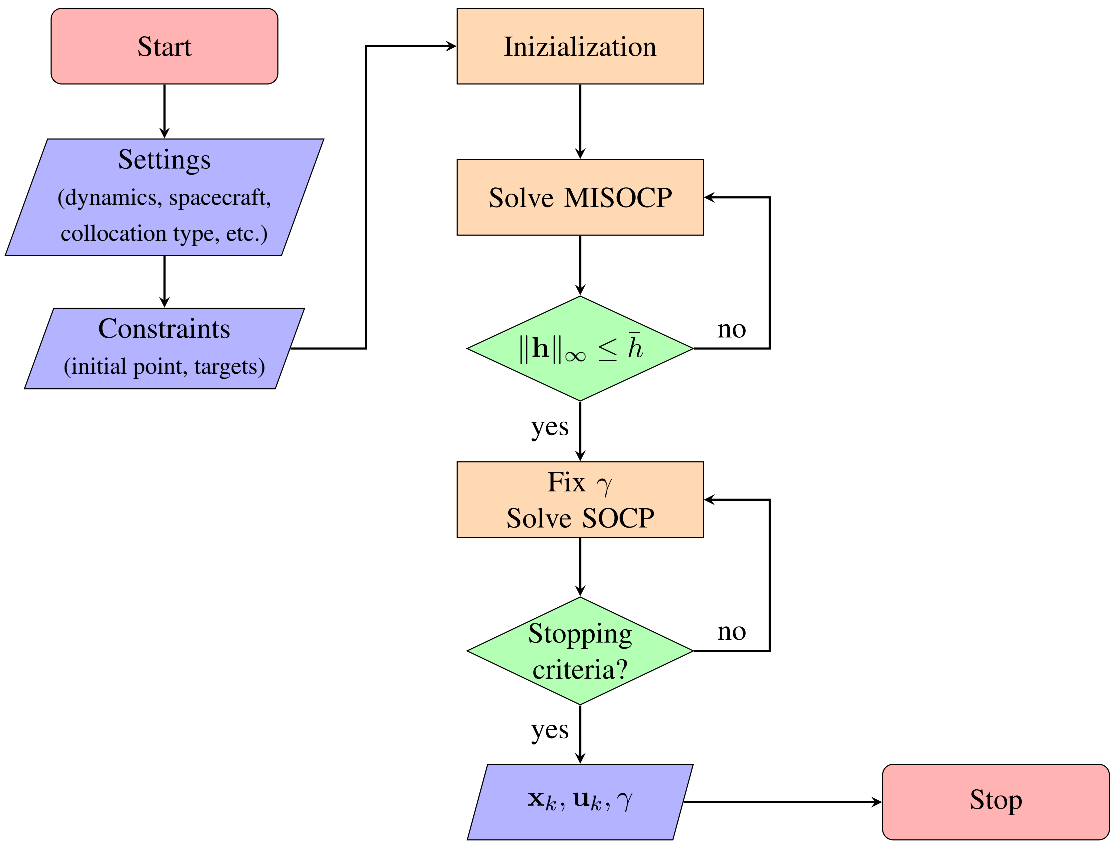

Figure 2: Sketch of the procedure to solve the goal-oriented fuel optimal problem.

Simulation overview

In order to test the algorithm presented in this work under diverse mission profiles in terms of spacecraft, target body, dynamics, and initial trajectory, two problems will be used as test case scenarios:

Table 1: SCP parameters

Parameter	Value
λ	100.0
M	10.0
R_0	100.0
(ρ_0, ρ_1, ρ_2)	$(0.01, 0.2, 0.85)$
(α, β)	$(1.5, 1.5)$
λ_{TR}	1000.0
τ	2.5
λ_g	$1/N_g$
$\bar{h}$	10^{-4}
$(\varepsilon_h, \varepsilon_z, \varepsilon_x, \varepsilon_R)$	$\left(10^{-6}, 10^{-4}, 10^{-8}, 10^{-4}\right)$

1) a CubeSat flying about a small asteroid in a Sun-stabilized terminator orbit (SSTO);

2) a SmallSat in a quasi-Keplerian orbit about a medium-sized asteroid.

For both the scenarios, the impact on computational time and convergence rate of the discretization method, (MI)SOCP solver, trust region approach, and target constraint approach is evaluated. To this aim, 20 simulations with random initial conditions and random targets (distributed uniformly on the target surface), and with the characteristic provided in Table 2 are performed. All the simulations are carried out in Julia on a 8-core Intel Core i7-10870H@2.20GHz laptop with 16 GB of RAM.

Table 2: Simulation parameters

Parameter	Value
Time of Flight	7 d
Initial time t_0	January 1, 2029
Number of goals N_g	7
Maximum runtime	500 s
Maximum iterations	50

Scenario 1 The first scenario is based on the ESA's mission SATIS.[48] SATIS is a 12XL CubeSat having the aim to reach the asteroid Apophis before its flyby with the Earth in 2029 and perform scientific activities to characterize the asteroid before and after its close encounter. In this case, the target is modeled as a tri-axial ellipsoid.[49] The CubeSat is considered to be placed on an SSTO, generated with the procedure in Takahashi and Scheeres,[50] and perturbed by the SRP and the gravitational perturbatons by the Sun, the Earth, and the Moon. This choice is common in CPOs close to minor bodies due to the stability of this kind of orbit in a high-perturbed environment, like the one of Apophis close to its close encounter.
Table 3 summarizes the main values of both target and spacecraft associated to this scenario.

Scenario 2 The second scenario investigates a SmallSat flying about (433)Eros. Eros is selected as target body since it is a medium-sized asteroid with a well known shape and used commonly in goal-oriented approaches.[27,52] In order to proper model the gravity related to its peculiar shape, the spherical harmonics model is used, considering also the SRP and the gravitational pulling by the Sun. On the other hand, the spacecraft is considered to be placed at the beginning on a perturbed circular orbit, since the main body is massive enough to have long-lasting quasi-Keplerian orbits. Spacecraft data are taken from the mission RAMSES.[22]
Table 4 summarizes the main values of both target and spacecraft associated to this scenario.

Table 3: Scenario 1 parameters. $\mathcal{U}$ indicates the uniform distribution.

	Parameter	Value
Spacecraft	Initial orbit semimajor axis a_0	$\mathcal{U}(0.6\,\mathrm{km}, 1.5\,\mathrm{km})$
	m_0	$25\,\mathrm{kg}$
	$T_{\max}$	$2\,\mathrm{mN}$
	I_{sp}	$1500\,\mathrm{s}$
	C_r	1.3
	A	$1.5\,\mathrm{m}^2$
Main body	Gravity type	Tri-axial ellipsoid
	μ	$2.736\,463 \times 10^{-9}\,\mathrm{km}^3/\mathrm{s}^2$
	(a, b, c)	$(228.966\,\mathrm{m}, 159.026\,\mathrm{m}, 139.798\,\mathrm{m})$ [49]
	ω	$283.46\,°/\mathrm{d}$ [51]
Goals	α	$20°$
	r_m	$0.5\,\mathrm{km}$
	r_M	$5\,\mathrm{km}$

Table 4: Scenario 2 parameters

	Parameter	Value
Spacecraft	Initial orbit position (x_0, y_0, z_0)	$(\mathcal{U}(45\,\mathrm{km}, 60\,\mathrm{km}), 0.0, \mathcal{U}(45\,\mathrm{km}, 60\,\mathrm{km}))$
	m_0	$500\,\mathrm{kg}$
	$T_{\max}$	$20\,\mathrm{mN}$
	I_{sp}	$1500\,\mathrm{s}$
	C_r	1.3
	A	$25\,\mathrm{m}^2$
Main body	Gravity type	Spherical harmonics
	μ	$4.463\,104 \times 10^{-4}\,\mathrm{km}^3/\mathrm{s}^2$ [53]
	Order and degree considered	Up to 8×8 [*]
	ω	$1639.46\,°/\mathrm{d}$ [54]
Goals	α	$10°$
	r_m	$5\,\mathrm{km}$
	r_M	$60\,\mathrm{km}$

Results

An example solution for both Scenario 1 and Scenario 2 are presented in Figs. 3 and 4, respectively, while Figs. 5 and 6 shows the simulations results. The time metric is the 90-th percentile of the converged solutions.
Generally speaking, it can be noted that the trends do not depend on the specific scenario. Convergence ratios are similar, while computational times are generally higher in the Scenario 2, although showing similar behaviors. Higher computational times are related to a higher number of branch-and-bound nodes that are visited in Scenario 2, while the number of iterations for the SCP is similar (i.e., a mean of 19.55 iterations in Scenario 1, against 20.15 for Scenario 2). The slower evaluation of the dynamics in Scenario 2 contributes to a lesser degree.
Regarding the discretization methods, low-order LGL and FOH exhibit the best balance in terms of convergence and runtime, while ZOH, even if faster, fails more frequently.
On the other hand, the use of the soft target approach can improve the convergence ratio. However, some of these solutions do not fulfill all the target constraints, thus the soft target approach allow to trade a higher convergence rate with a lower number of satisfied targets. This approach can be exploited to maximize the scientific output, avoiding unfeasible solutions. This aspect is deepened in the next section.

Figure 7 shows a Pareto front, varying the number of targets. For each selected number of targets, 20 simulations of Scenario 1 exploiting FOH and a hard trust region approach are considered. Each point represents the 95-th percentile, while the bars encompass the result of all the converged solutions. As expected, the propellant mass needed increases as the number of target increases. However, it could be noted also that the number of converged solutions decrease with the required targets to be fulfilled.

ADDITIONAL FORMULATIONS

Problem 3 can be easily extended and modified to change the behavior of the problem or to add additional constraints. These modifications can be implemented both to improve the model or to fulfill system requirements. Some examples are reported in the remainder of this section.

Targets database

When considering a realistic scenario, a mission usually must not accomplished all the target goals, but a database of possible targets is provided by the scientific community and the goal becomes to maximize the scientific return by visiting the most number of them. In this case, Problem 3 can be modified to consider the target database. Specifically, the cost function will exploit a soft-goal approach, as in Eq. (43), i.e.,

$$\hat{J} = J - \lambda_g \sum_{i=1}^{N_g} \min\left(1, \sum_{k=0}^{N} \gamma_{i,k}\right)$$

while Eq. (22d) is removed, since that it is not required anymore that every target must be accomplished.
Figure 8 shows an example of a trajectory considering a database with 12 targets for the Scenario 1. In this case, only 9 targets could be satisfied. The computational time increases to $356\,\mathrm{s}$, mainly due to a more extended search in the branch-and-bound algorithm. This is related to the fact that,

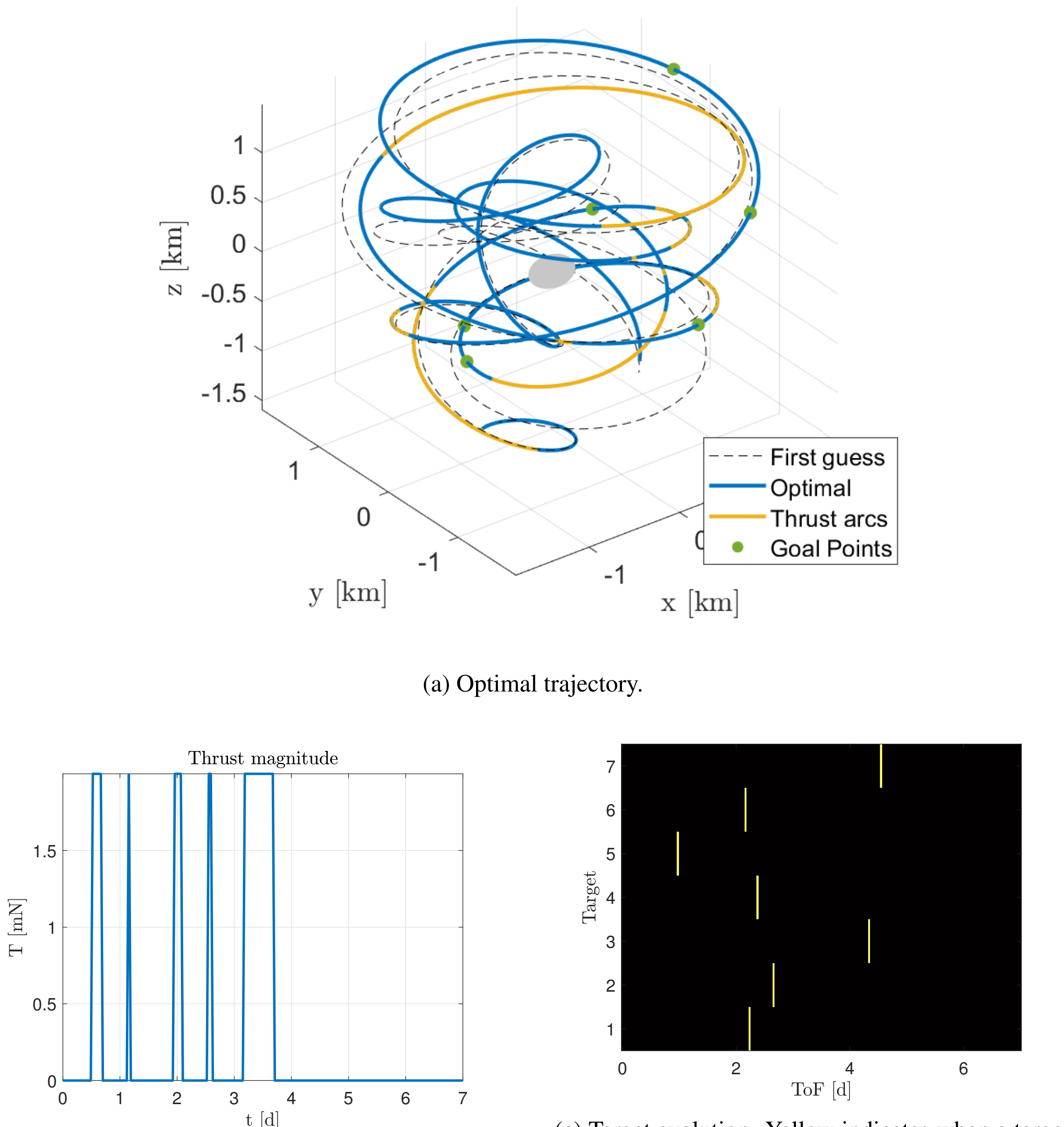

(a) Optimal trajectory.

(b) Control profile.

(c) Target evolution. Yellow indicates when a target is respected.

Figure 3: Scenario 1 solution example.

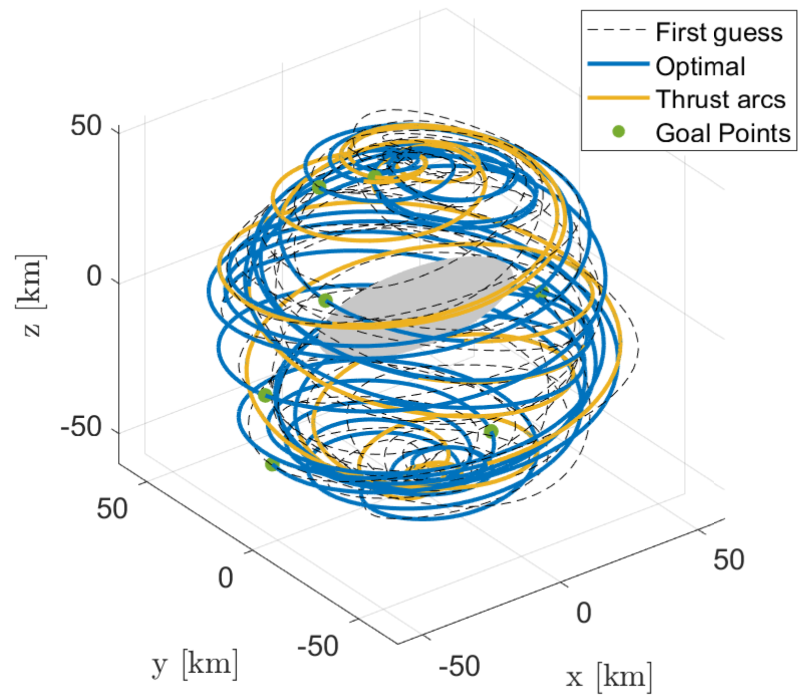

(a) Optimal trajectory.

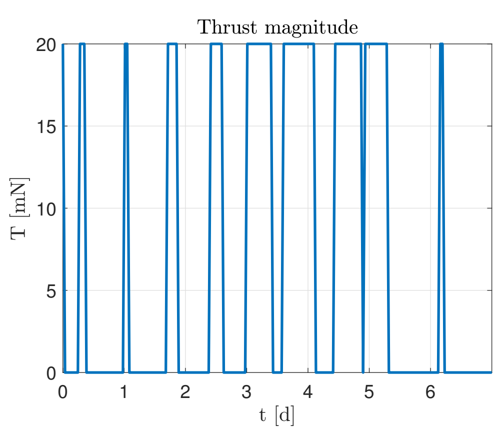

(b) Control profile.

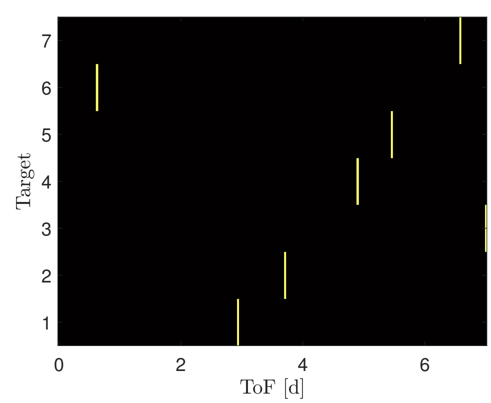

(c) Target evolution. Yellow indicates when a target is respected.

Figure 4: Scenario 2 solution example.

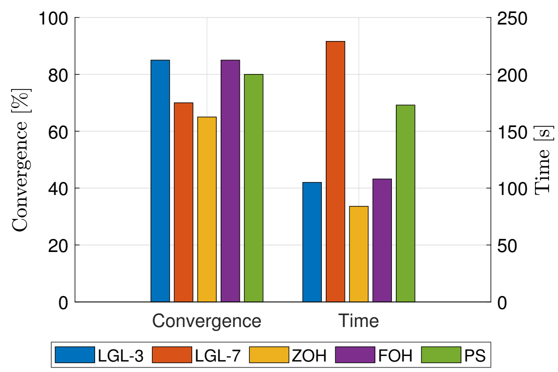

(a) Comparison of different discretization methods.

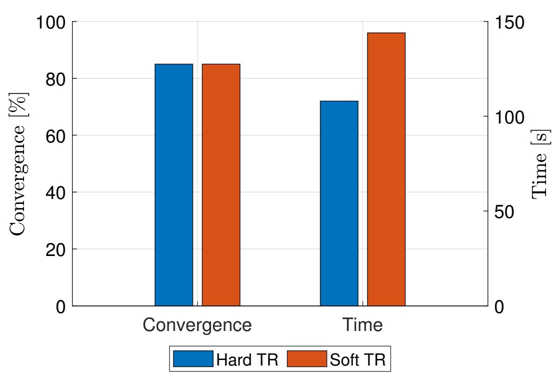

(b) Hard vs soft trust region approach.

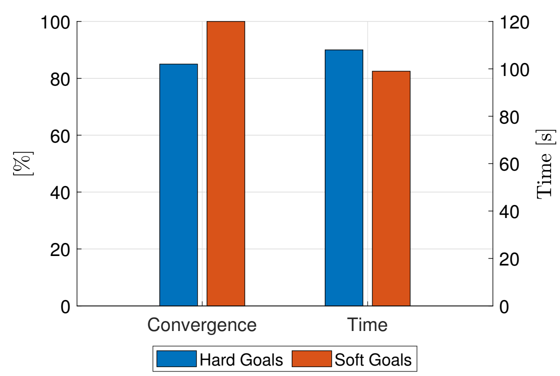

(c) Hard vs soft target constraints approach.

Figure 5: Scenario 1 results.

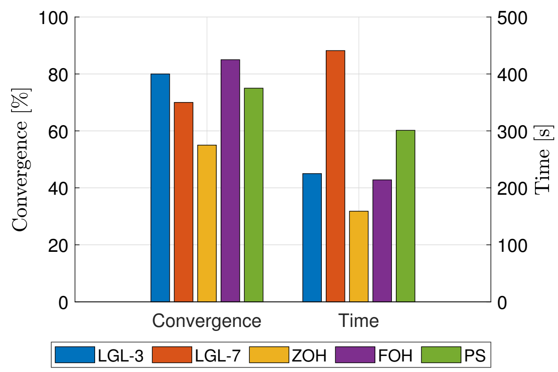

(a) Comparison of different discretization methods.

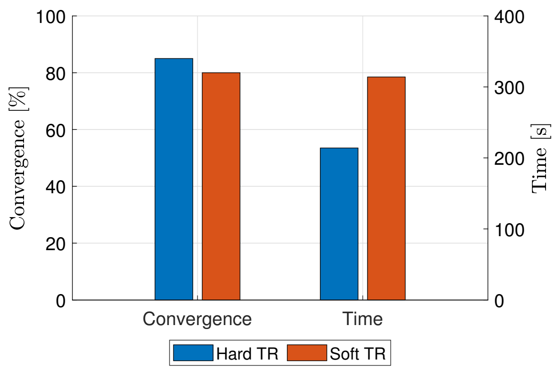

(b) Hard vs soft trust region approach.

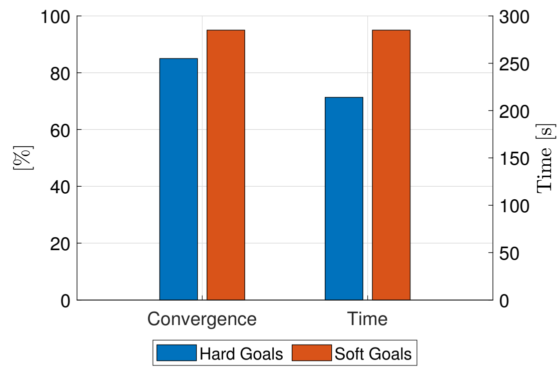

(c) Hard vs soft target constraints approach.

Figure 6: Scenario 2 results.

considering a database, the algorithm has to select not only when a target is satisfied but also the subset of targets to be visited. From a more practical point of view, in the original formulation, the algorithm is aware that for each row of the variable γ at least one element must be 1. In this case, on the contrary, there is not such a constraint (i.e., a row can be null), increasing so the search space.

Additional constraints

On the other hand, additional constraints can be added easily. For example, it must be required to look at targets with certain illumination conditions, i.e., with the phase angle below a prescribed threshold. In this case,

$$\gamma_{i,k} \leq \left(1 - \left(\cos\beta - \frac{\mathbf{r}_{S,k}^T \mathbf{r}_{c_i}}{\|\mathbf{r}_{S,k}\| \|\mathbf{r}_{c_i}\|}\right)\right) \qquad \text{for } k = 0, \ldots, N, \quad \text{for } i = 1, \ldots, N_g \tag{44}$$

where $\mathbf{r}_{S,k}$ is the position of the Sun at the node k and β is the desired phase angle threshold. Eq. (44) forces $\gamma_{i,k}$ to be null if the desired phase angle is not attained.
Due to attitude constraint it is usually not possible to look at two targets at the same time. This

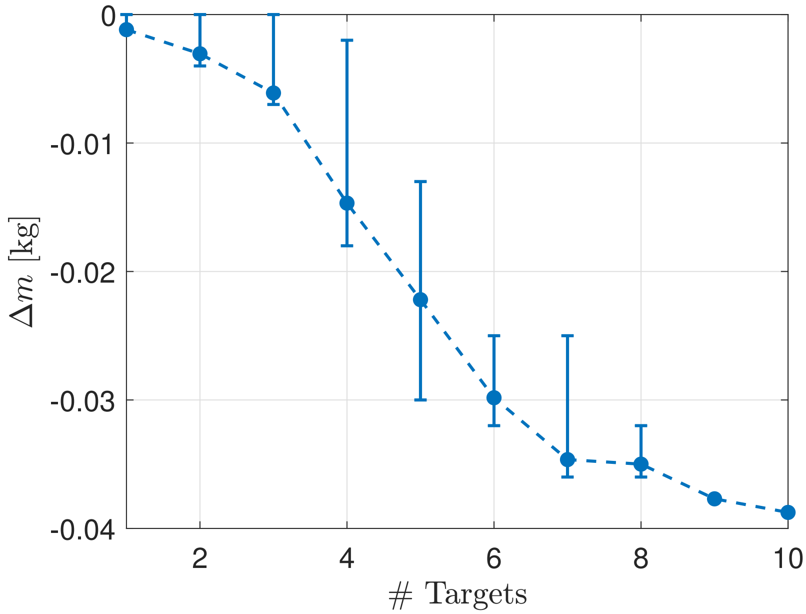

Figure 7: Pareto front of Scenario 1 considering a different number of targets in the database. Each point considers 20 simulations.

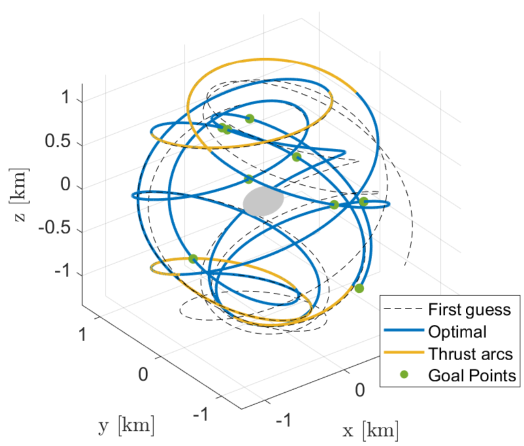

(a) Optimal trajectory.

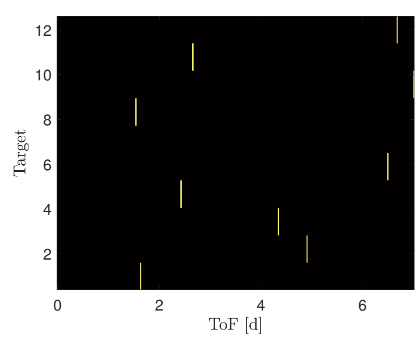

(b) Target evolution. Yellow indicates when a target is respected.

Figure 8: Solution example considering target database.

constraint may be formulated as,

$$\sum_{i=1}^{N_g} \gamma_{i,k} \leq 1 \qquad \text{for } k = 0, \dots, N \tag{45}$$

meaning that at each time at maximum one target constraint could be counted.
Another possibility is to impose a no-thrust arc when looking at the target. As a matter of fact, in a realistic scenario, it is not desirable to operate the engine when performing scientific observations, due to attitude constraints and possible on-board resources limitations. In this case, the additional constraint

$$\Gamma_k \leq M \left(1 - \sum_{i=1}^{N_g} \gamma_{i,k}\right) \qquad \text{for } k = 0, \dots, N \tag{46}$$

must be added, that forces the thrust to be null when at least one target is observed. Applying the same constraint to neighboring nodes can be used to extend the no-thrust arc, mimicking the requirement to avoid thrust when performing a slew, necessary when transitioning from body pointing to maneuver-direction pointing, and vice versa.
All these additional constraints are also in principle able to reduce the computational times, since they tighten the model, i.e., they remove branches and nodes in the branch-and-bound algorithm.
A trajectory example is provided in Fig. 9. This example, based on Scenario 1, considers a phase angle threshold $\beta = 90\,\mathrm{deg}$, i.e., it is sufficient for the target to be illuminated, and a $1.5\,\mathrm{h}$ no-trust constraint before and after each observation. The same 12-target database of Fig. 8 is used to allow a simpler comparison. In this case, only 6 targets are satisfied, with the trajectory being completely different from the one in Fig. 8, mainly due to the phase angle constraint. From Fig. 9b, the no-thrust arcs about observations 1 and 2 can be noted.

CONCLUSION

In this work, a novel algorithm to compute goal-oriented fuel-optimal trajectories for low-thrust spacecraft about minor bodies is introduced. The methodology is based on sequential convex problem. Under the SCP framework, the nonlinear problem is translated in a mixed-integer second-order cone constraint problem, that is solved iteratively to find the optimal trajectory. Numerical simulations on two different scenarios are used to evaluate convergence and computational effort and to assess the impact on the performances of discretization method, trust region approach, and target constraint approach. No significant difference is found between the two test cases for the other parameters under evaluation. Converge rate and computational times are better in case of low-order LGL or FOH, hard trust region constraint, and a two-phase algorithm combining some steps of the MISOCP, followed by the simple SOCP to refine the best solution. In this case, the algorithm is able to provide optimal solutions in about 200 and 300 seconds for the two scenarios, respectively, with a convergence rate of more than the 80%. Alternative formulations considering a target database, or constraints on the phase angle, number of observations per node, and no-thrust arcs when performing scientific activities are presented and tested.
Even though this work does not present a convergence proof, the high percentage of converged cases has shown that SCP is very reliable and it seems to be a viable method to compute goal-oriented low-thrust trajectories.

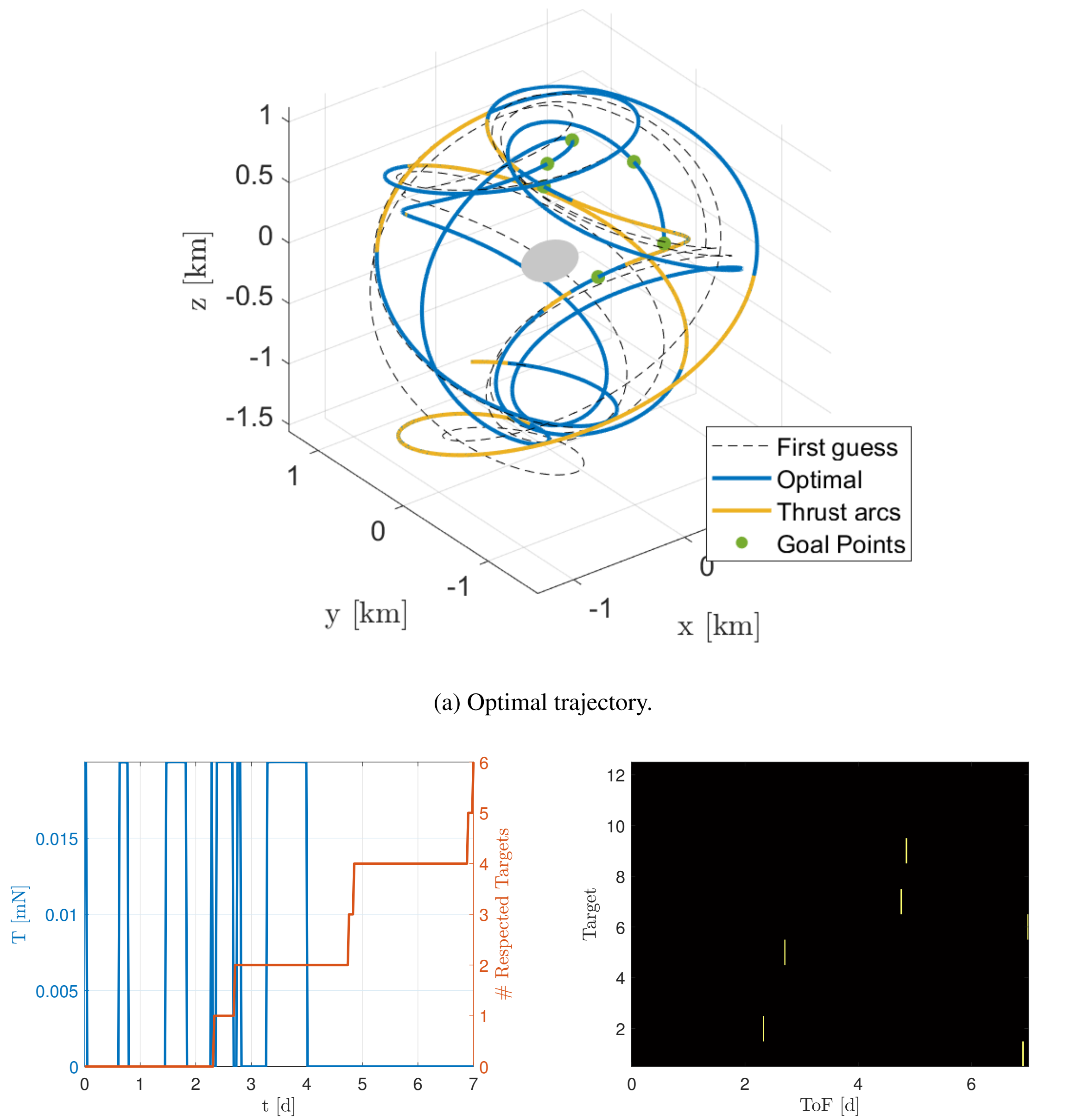

(a) Optimal trajectory.

(b) Control profile with the target cumulative number.

(c) Target evolution. Yellow indicates when a target is respected.

Figure 9: Alternative formulation solution example.

ACKNOWLEDGMENT

This project is part of CASTOR, a project that has received funding from the European Union's Horizon Europe research and innovation programme under the Marie Skłodowska-Curie grant agreement no. 101103826.
Part of this research was carried out at the Jet Propulsion Laboratory, California Institute of Technology, under a contract with the National Aeronautics and Space Administration (80NM0018D0004).
C.G. would like to thank Christian Hofmann and Andrea Carlo Morelli for the fruitful discussions and suggestions about sequential convex programming.

REFERENCES

[1] J. Oro, T. Mills, and A. Lazcano, "Comets and life in the universe," *Advances in Space Research*, Vol. 15, No. 3, 1995, pp. 81–90.

[2] E. Asphaug, "Growth and evolution of asteroids," *Annual Review of Earth and Planetary Sciences*, Vol. 37, No. 1, 2009, pp. 413–448.

[3] A. Hein, M. Saidani, and H. Tollu, "Exploring Potential Environmental Benefits of Asteroid Mining," *69th International Astronautical Congress (IAC), Bremen, Germany, 1–5 October 2018*, 2018.

[4] C. R. Chapman, "The hazard of near-Earth asteroid impacts on earth," *Earth and Planetary Science Letters*, Vol. 222, No. 1, 2004, pp. 1–15.

[5] S. B. A. G. (SBAG), *Goals and Objectives for the Exploration and Investigation of the Solar System's Small Bodies*.

[6] J. C. Castillo-Rogez, M. Pavone, J. A. Hoffman, and I. A. Nesnas, "Expected science return of spatially-extended in-situ exploration at small solar system bodies," *2012 IEEE Aerospace Conference*, IEEE, 2012, pp. 1–15.

[7] D. Lauretta, S. Balram-Knutson, E. Beshore, W. Boynton, C. Drouet d'Aubigny, D. DellaGiustina, H. Enos, D. Golish, C. Hergenrother, E. Howell, *et al.*, "OSIRIS-REx: sample return from asteroid (101955) Bennu," *Space Science Reviews*, Vol. 212, 2017, pp. 925–984.

[8] S.-i. Watanabe, Y. Tsuda, M. Yoshikawa, S. Tanaka, T. Saiki, and S. Nakazawa, "Hayabusa2 mission overview," *Space Science Reviews*, Vol. 208, 2017, pp. 3–16.

[9] L. Prockter, S. Murchie, A. Cheng, S. Krimigis, R. Farquhar, A. Santo, and J. Trombka, "The NEAR shoemaker mission to asteroid 433 eros," *Acta Astronautica*, Vol. 51, No. 1-9, 2002, pp. 491–500.

[10] D. Brownlee, "The Stardust mission: analyzing samples from the edge of the solar system," *Annual Review of Earth and Planetary Sciences*, Vol. 42, No. 1, 2014, pp. 179–205.

[11] K.-H. Glassmeier, H. Boehnhardt, D. Koschny, E. Kührt, and I. Richter, "The Rosetta mission: flying towards the origin of the solar system," *Space Science Reviews*, Vol. 128, 2007, pp. 1–21.

[12] P. Lord, S. Tilley, D. Y. Oh, D. Goebel, C. Polanskey, S. Snyder, G. Carr, S. M. Collins, G. Lantoine, D. Landau, *et al.*, "Psyche: Journey to a metal world," *2017 IEEE Aerospace Conference*, IEEE, 2017, pp. 1–11.

[13] M. Kueppers, P. Martino, I. Carnelli, and P. Michel, "Ramses–ESA's Study for a Small Mission to Apophis," *AAS/Division for Planetary Sciences Meeting Abstracts*, Vol. 55, 2023, pp. 201–08.

[14] A. F. Cheng, A. S. Rivkin, P. Michel, J. Atchison, O. Barnouin, L. Benner, N. L. Chabot, C. Ernst, E. G. Fahnestock, M. Kueppers, *et al.*, "AIDA DART asteroid deflection test: Planetary defense and science objectives," *Planetary and Space Science*, Vol. 157, 2018, pp. 104–115.

[15] N. L. Chabot, A. S. Rivkin, A. F. Cheng, O. S. Barnouin, E. G. Fahnestock, D. C. Richardson, A. M. Stickle, C. A. Thomas, C. M. Ernst, R. T. Daly, *et al.*, "Achievement of the planetary defense investigations of the Double Asteroid Redirection Test (DART) mission," *The Planetary Science Journal*, Vol. 5, No. 2, 2024, p. 49.

[16] P. Michel, M. Küppers, A. C. Bagatin, B. Carry, S. Charnoz, J. De Leon, A. Fitzsimmons, P. Gordo, S. F. Green, A. Hérique, *et al.*, "The ESA Hera mission: detailed characterization of the DART impact outcome and of the binary asteroid (65803) Didymos," *The planetary science journal*, Vol. 3, No. 7, 2022, p. 160.

[17] A. Poghosyan and A. Golkar, "CubeSat evolution: Analyzing CubeSat capabilities for conducting science missions," *Progress in Aerospace Sciences*, Vol. 88, 2017, pp. 59–83, 10.1016/j.paerosci.2016.11.002.

[18] R. Walker, D. Binns, C. Bramanti, M. Casasco, P. Concari, D. Izzo, D. Feili, P. Fernandez, J. G. Fernandez, P. Hager, *et al.*, "Deep-space CubeSats: thinking inside the box," *Astronomy & Geophysics*, Vol. 59, No. 5, 2018, pp. 24–30, 10.1093/astrogeo/aty232.

[19] E. Dotto, V. Della Corte, M. Amoroso, I. Bertini, J. R. Brucato, A. Capannolo, B. Cotugno, G. Cremonese, V. Di Tana, I. Gai, *et al.*, "LICIACube-the Light Italian Cubesat for Imaging of Asteroids in support of the NASA DART mission towards asteroid (65803) Didymos," *Planetary and Space Science*, Vol. 199, 2021, p. 105185.

[20] H. R. Goldberg, Ö. Karatekin, B. Ritter, A. Herique, P. Tortora, C. Prioroc, B. G. Gutierrez, P. Martino, and I. Carnelli, "The juventas CubeSat in support of ESA's hera mission to the asteroid didymos," 2019.

[21] F. Ferrari, V. Franzese, M. Pugliatti, C. Giordano, and F. Topputo, "Preliminary mission profile of Hera's Milani CubeSat," *Advances in Space Research*, Vol. 67, No. 6, 2021, pp. 2010–2029.

[22] A. C. Morelli, A. Mannocchi, C. Giordano, F. Ferrari, and F. Topputo, "Initial Trajectory Assessment of a low-thrust option for the RAMSES Mission to (99942) Apophis," *Advances in Space Research*, Vol. 73, No. 8, 2024, pp. 4241–4253.

[23] S. Campagnola, N. Ozaki, Y. Sugimoto, C. H. Yam, H. Chen, Y. Kawabata, S. Ogura, B. Sarli, Y. Kawakatsu, R. Funase, *et al.*, "Low-thrust trajectory design and operations of PROCYON, the first deep-space micro-spacecraft," *25th International Symposium on Space Flight Dynamics*, Vol. 7, German Aerospace Center (DLR) Munich, Germany, 2015.

[24] F. Ferrari, V. Franzese, M. Pugliatti, C. Giordano, and F. Topputo, "Trajectory options for hera's milani cubesat around (65803) didymos," *The Journal of the Astronautical Sciences*, Vol. 68, No. 4, 2021, pp. 973–994.

[25] A. Accomazzo, P. Ferri, S. Lodiot, J.-L. Pellon-Bailon, A. Hubault, R. Porta, J. Urbanek, R. Kay, M. Eiblmaier, and T. Francisco, "Rosetta operations at the comet," *Acta Astronautica*, Vol. 115, 2015, pp. 434–441.

[26] P. G. Antreasian, C. D. Adam, K. Berry, J. Geeraert, K. M. Getzandanner, D. Highsmith, J. M. Leonard, E. J. Lessac-Chenen, A. H. Levine, J. V. McAdams, *et al.*, "OSIRIS-REx Proximity Operations and Navigation Performance at Bennu," *AIAA SCITECH 2022 Forum*, 2022, p. 2470.

[27] D. A. Surovik and D. J. Scheeres, "Adaptive reachability analysis to achieve mission objectives in strongly non-keplerian systems," *Journal of Guidance, Control, and Dynamics*, Vol. 38, No. 3, 2015, pp. 468–477.

[28] F. Capolupo, T. Simeon, and J.-C. Berges, "Heuristic guidance techniques for the exploration of small celestial bodies," *IFAC-PapersOnLine*, Vol. 50, No. 1, 2017, pp. 8279–8284.

[29] A. Rizza, C. Giordano, and F. Topputo, "A goal-oriented guidance approach for binary asteroids exploration," *Astrodynamics*, 2024. In press.

[30] D. Malyuta, T. P. Reynolds, M. Szmuk, T. Lew, R. Bonalli, M. Pavone, and B. Açıkmeşe, "Convex optimization for trajectory generation: A tutorial on generating dynamically feasible trajectories reliably and efficiently," *IEEE Control Systems Magazine*, Vol. 42, No. 5, 2022, pp. 40–113.

[31] B. Acikmese and S. R. Ploen, "Convex programming approach to powered descent guidance for mars landing," *Journal of Guidance, Control, and Dynamics*, Vol. 30, No. 5, 2007, pp. 1353–1366.

[32] C. Hofmann and F. Topputo, "Rapid low-thrust trajectory optimization in deep space based on convex programming," *Journal of Guidance, Control, and Dynamics*, Vol. 44, No. 7, 2021, pp. 1379–1388.

[33] C. Hofmann, A. C. Morelli, and F. Topputo, "Performance assessment of convex low-thrust trajectory optimization methods," *Journal of Spacecraft and Rockets*, Vol. 60, No. 1, 2023, pp. 299–314.

[34] D. J. Scheeres, "Dynamics about uniformly rotating triaxial ellipsoids: applications to asteroids," *Icarus*, Vol. 110, No. 2, 1994, pp. 225–238.

[35] G. Balmino, "Gravitational potential harmonics from the shape of an homogeneous body," *Celestial Mechanics and Dynamical Astronomy*, Vol. 60, 1994, pp. 331–364.

[36] Z. Wang and M. J. Grant, "Minimum-fuel low-thrust transfers for spacecraft: A convex approach," *IEEE Transactions on Aerospace and Electronic Systems*, Vol. 54, No. 5, 2018, pp. 2274–2290.

[37] D. Malyuta, T. Reynolds, M. Szmuk, M. Mesbahi, B. Acikmese, and J. M. Carson, "Discretization performance and accuracy analysis for the rocket powered descent guidance problem," *AIAA Scitech 2019 Forum*, 2019, p. 0925.

[38] J. T. Betts, "Survey of numerical methods for trajectory optimization," *Journal of guidance, control, and dynamics*, Vol. 21, No. 2, 1998, pp. 193–207.

[39] P. Williams, "Hermite-Legendre-Gauss-Lobatto direct transcription in trajectory optimization," *Journal of guidance, control, and dynamics*, Vol. 32, No. 4, 2009, pp. 1392–1395.

[40] C. Zhang, F. Topputo, F. Bernelli-Zazzera, Y.-S. Zhao, *et al.*, "An exploration of numerical methods for low-thrust trajectory optimization in nbody models," *Proceedings of International Astronautical Congress, Beijing, China*, 2013, pp. 23–27.

[41] K. Subbarao and B. M. Shippey, "Hybrid genetic algorithm collocation method for trajectory optimization," *Journal of Guidance, Control, and Dynamics*, Vol. 32, No. 4, 2009, pp. 1396–1403.

[42] A. C. Morelli, C. Hofmann, and F. Topputo, "Robust low-thrust trajectory optimization using convex programming and a homotopic approach," *IEEE Transactions on Aerospace and Electronic Systems*, Vol. 58, No. 3, 2021, pp. 2103–2116.

[43] I. M. Ross and M. Karpenko, "A review of pseudospectral optimal control: From theory to flight," *Annual Reviews in Control*, Vol. 36, No. 2, 2012, pp. 182–197.

[44] F. Fahroo and I. M. Ross, "Direct trajectory optimization by a Chebyshev pseudospectral method," *Journal of Guidance, Control, and Dynamics*, Vol. 25, No. 1, 2002, pp. 160–166.

[45] G. Tang, F. Jiang, and J. Li, "Fuel-optimal low-thrust trajectory optimization using indirect method and successive convex programming," *IEEE Transactions on Aerospace and Electronic Systems*, Vol. 54, No. 4, 2018, pp. 2053–2066.

[46] C. C. Françolin, D. A. Benson, W. W. Hager, and A. V. Rao, "Costate approximation in optimal control using integral Gaussian quadrature orthogonal collocation methods," *Optimal Control Applications and Methods*, Vol. 36, No. 4, 2015, pp. 381–397.

[47] M. Udell, K. Mohan, D. Zeng, J. Hong, S. Diamond, and S. Boyd, "Convex Optimization in Julia," *SC14 Workshop on High Performance Technical Computing in Dynamic Languages*, 2014.

[48] R. Walker, "Overview of ESA Lunar & Interplanetary CubeSat Missions," *Interplanetary Small Satellite Conference*, 2023.

[49] G. Valvano, O. C. Winter, R. Sfair, R. Machado Oliveira, G. Borderes-Motta, and T. Moura, "APOPHIS–effects of the 2029 Earth's encounter on the surface and nearby dynamics," *Monthly Notices of the Royal Astronomical Society*, Vol. 510, No. 1, 2022, pp. 95–109.

[50] S. Takahashi and D. J. Scheeres, "Higher-order corrections for frozen terminator orbit design," *Journal of Guidance, Control, and Dynamics*, Vol. 43, No. 9, 2020, pp. 1642–1655.

[51] P. Pravec, P. Scheirich, J. Ďurech, J. Pollock, P. Kušnirák, K. Hornoch, A. Galad, D. Vokrouhlickỳ, A. Harris, E. Jehin, *et al.*, "The tumbling spin state of (99942) Apophis," *Icarus*, Vol. 233, 2014, pp. 48–60.

[52] A. Rizza, F. Topputo, and S. D'Amico, "Goal-oriented asteroid mapping under uncertainties using Sequential Convex Programming," *AIAA Scitech 2024 Forum*, 2024, p. 1990.

[53] D. Yeomans, P. Antreasian, J.-P. Barriot, S. Chesley, D. Dunham, R. Farquhar, J. Giorgini, C. Helfrich, A. Konopliv, J. McAdams, *et al.*, "Radio science results during the NEAR-Shoemaker spacecraft rendezvous with Eros," *Science*, Vol. 289, No. 5487, 2000, pp. 2085–2088.

[54] J. K. Miller, A. Konopliv, P. Antreasian, J. Bordi, S. Chesley, C. Helfrich, W. Owen, T. Wang, B. Williams, D. Yeomans, *et al.*, "Determination of shape, gravity, and rotational state of asteroid 433 Eros," *Icarus*, Vol. 155, No. 1, 2002, pp. 3–17.